Research Article

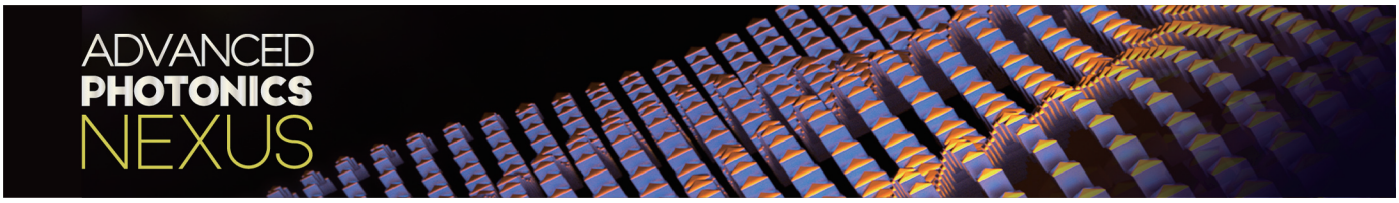

Single-wavelength size focusing of ultra-intense ultrashort lasers with rotational hyperbolic mirrors

Zhaoyang Li,[a,b,*] **Yanqi Liu**,[a] **Xiaoyang Guo**,[c] **Yuxin Leng**,[b] **and Ruxin Li**[a,b,d]

[a]Zhangjiang Laboratory, Shanghai, China
[b]Chinese Academy of Sciences, Shanghai Institute of Optics and Fine Mechanics, Key Laboratory of Ultra-intense Laser Science and Technology, Shanghai, China
[c]Shenzhen Technology University, College of Engineering Physics, Shenzhen, China
[d]ShanghaiTech University, Shanghai, China

Abstract. Compressing all the energy of a laser pulse into a spatiotemporal focal cube edged by the laser center wavelength will realize the highest intensity of an ultra-intense ultrashort laser, which is called the λ^3 regime or the λ^3 laser. Herein, we introduced a rotational hyperbolic mirror—an important rotational conic section mirror with two foci—that is used as a secondary focusing mirror after a rotational parabolic mirror to reduce the focal spot size from several wavelengths to a single wavelength by significantly increasing the focusing angular aperture. Compared with the rotational ellipsoidal mirror, the first focal spot with a high intensity, as well as some unwanted strong-field effects, is avoided. The optimal focusing condition of this method is presented and the enhanced tight focusing for a femtosecond petawatt laser and the λ^3 laser is numerically simulated, which can enhance the focused intensities of ultra-intense ultrashort lasers for laser physics.

Keywords: ultra-intense ultrashort lasers; beam focusing; focused intensity; hyperbolic mirrors.

Received Jan. 30, 2024; revised manuscript received Feb. 29, 2024; accepted for publication Mar. 11, 2024; published online Mar. 29, 2024.

[DOI: 10.1117/1.APN.3.3.036002]

1 Introduction

Strong-field laser physics[1] and ultrafast laser physics[2] are currently important research areas in experimental physics. Focused intensity, rather than unfocused peak power, is the parameter of most interest in both strong-field and ultrafast laser physics, and it largely determines whether the goals of a physics experiment can be achieved. The highest intensity of an ultra-intense ultrashort laser facility, recently called a femtosecond petawatt laser (fs-PW), is approximately the value when all the pulse energy is contained within a spatiotemporal focal cube edged by the laser center wavelength, i.e., a single-optical-cycle pulse and a single-wavelength-sized focal spot are obtained at the same time, which is called the λ^3 regime or the λ^3 laser by Mourou et al.[1,3] In the time domain, single-cycle and even subcycle optical pulses have been realized in both near- and mid-infrared wavelengths by optical parametric amplification (OPA),[4,5] optical parametric chirped pulse amplification (OPCPA),[6] coherent waveform/spectrum synthesis,[7] nonlinear postcompression,[8–11] etc., in low-energy lasers, and recently some improved OPAs/OPCPAs have also been proposed for high-energy lasers, e.g., single-cycle petawatt-class lasers.[12–15] In the space domain, near-single-wavelength-sized focal spots have been produced by tight-focusing optics with small f-numbers in some low-energy lasers. A recent reported result in a high-energy laser is that a 1.1 μm [full width at half-maximum (FWHM)] near diffraction-limited spot size was achieved in a 4-petawatt laser by an $f/1.1$ ($f = 300$ mm) off-axis parabolic mirror and deformable mirrors for the realization of a 10^{23} W/cm^2 intensity.[16] Typically, large-aperture tight focusing elements with very small f-numbers (e.g., meter-sized $f/\sim 1$ off-axis parabolic mirrors) are very difficult to fabricate and very hard to adjust to near-ideal conditions, which is not conducive to obtaining very small focal spots in experiments. To solve this

*Address all correspondence to Zhaoyang Li, lizy@zjlab.ac.cn

problem, the ellipsoidal mirror (or ellipsoidal plasma mirror) with two foci is used as a secondary focusing mirror after a parabolic mirror to further reduce the focal spot size by shifting its location from one focus to another, and a one-fifth reduction of two near-diffraction-limited focal spots from about 4.5 to 0.9 μm (FWHM) was demonstrated in experiments.[17,18] As a secondary focusing mirror, the ellipsoidal mirror can magnify the output focusing angular aperture at the second focus compared to the input focusing angular aperture at the first focus, thereby producing a smaller focal spot. However, the high intensity at the first focus can generate some unwanted strong-field effects, e.g., ionization of a nonideal vacuum.[19] In geometry, the bifocal conic section includes not only ellipses but also hyperbolas.

In this article, we propose a method to use a rotational hyperbolic mirror as a secondary focusing mirror after a rotational parabolic mirror to reduce the focal spot size to a single wavelength. We have investigated the magnification of the focusing angular aperture of hyperbolic mirrors, proposed the optimal focusing conditions, and simulated the results in the fs-PW and λ^3 lasers, which contribute to the realization of ultra-intense ultrashort lasers with the highest intensities for extreme strong-field physics.

2 Results

2.1 Angular Aperture Magnification

In a strong-field or ultrafast laser physics experiment, a rotational parabolic mirror focuses a collimated laser beam to its focus, where an experimental target is located for light–matter interactions. Figure 1(a) shows that when a rotational hyperbolic mirror is introduced, with one of its foci located at the focus of the rotational parabolic mirror, the reflected beam will be focused at its other focus, where the focusing angular aperture will be enlarged, resulting in a smaller focal spot. Figure 1(b) shows a profile containing the reflection and focusing processes, and a Cartesian coordinate system of x-y-z is set up with reflections in the x-z plane and two foci on the z axis and symmetric about the x axis. The input and output angular semi-apertures are $\Delta\alpha$ and $\Delta\alpha'$, which are located at the input and output foci $F_1(-c,0)$ and $F_2(c,0)$, respectively. The semi-major axis of the hyperbola is a, and the eccentricity is c/a, which is larger than 1 for hyperbolas. The angle between the edge of the beam and the z axis is defined as the edge angle α_e, which should be larger than zero to avoid the experiment target blocking the input beam. For comparison, Fig. 1(c) shows the secondary focusing using a rotational ellipsoidal mirror, where the two foci of the ellipse have the same locations: $F_1(-c,0)$ and $F_2(c,0)$. The semi-major axis of the ellipse is a, and the eccentricity c/a is smaller than 1 for ellipses.

Using the calculation model given in Appendix A, the angular apertures at the two foci are calculated for different cases. Figures 2(a) and 2(b) show the variation of the magnification ratio $\Delta\alpha'/\Delta\alpha$ and the output angular aperture $2\Delta\alpha'$ with different eccentricities c/a, respectively. The edge angle is fixed at $\alpha_e = 5$ deg and the results are given for three input angular apertures of $2\Delta\alpha = 10$ deg, 20 deg, and 30 deg. The calculations show that, first, the angular aperture can be increased by optimizing the eccentricity c/a; second, there exists an optimal eccentricity c/a_{opt} for both ellipses ($0 < c/a < 1$) and hyperbolas ($c/a > 1$), which corresponds to an optimal magnification ratio $\Delta\alpha'_{\text{opt}}/\Delta\alpha$ and an optimal output angular aperture $2\Delta\alpha'_{\text{opt}}$ with the maximum values. It can be found that for the same input (i.e., the same input angular aperture $2\Delta\alpha$ and the same edge angle α_e), the optimal magnification ratio $\Delta\alpha'_{\text{opt}}/\Delta\alpha$ and the optimal output angular aperture $2\Delta\alpha'_{\text{opt}}$ is the same for both ellipses and hyperbolas. Table 1 gives the optimal focusing conditions for both ellipses and hyperbolas, when the edge angle is $\alpha_e = 5$ deg and the input angular apertures are $2\Delta\alpha = 10$ deg, 20 deg, and 30 deg. In addition, Fig. 2(a) shows that the magnification ratio $\Delta\alpha'/\Delta\alpha$ increases as the input angular aperture

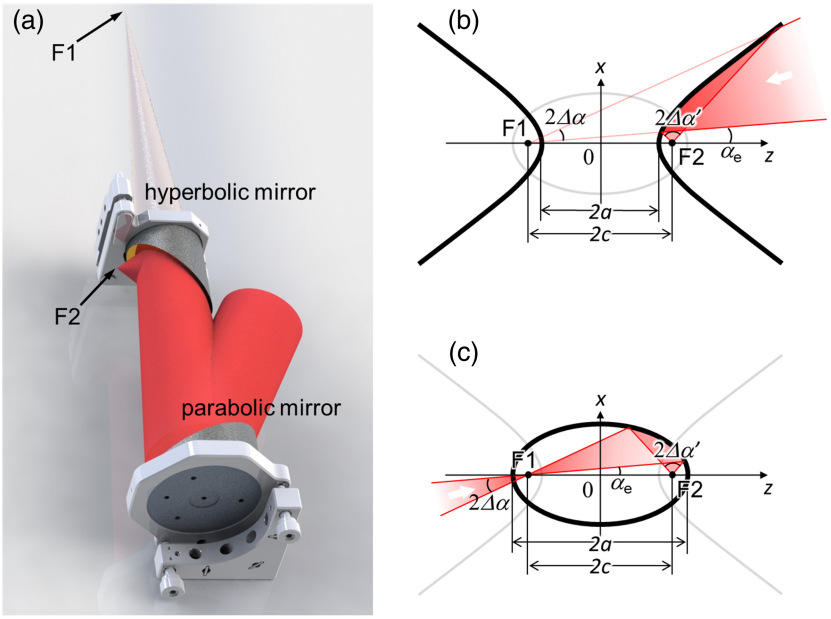

Fig. 1 (a) Schematic of tight focusing using a parabolic mirror and a hyperbolic mirror. Illustration and comparison of secondary focusing using (b) hyperbolic and (c) ellipsoidal mirrors. $2\Delta\alpha$ and $2\Delta\alpha'$ are input and output angular apertures, respectively.

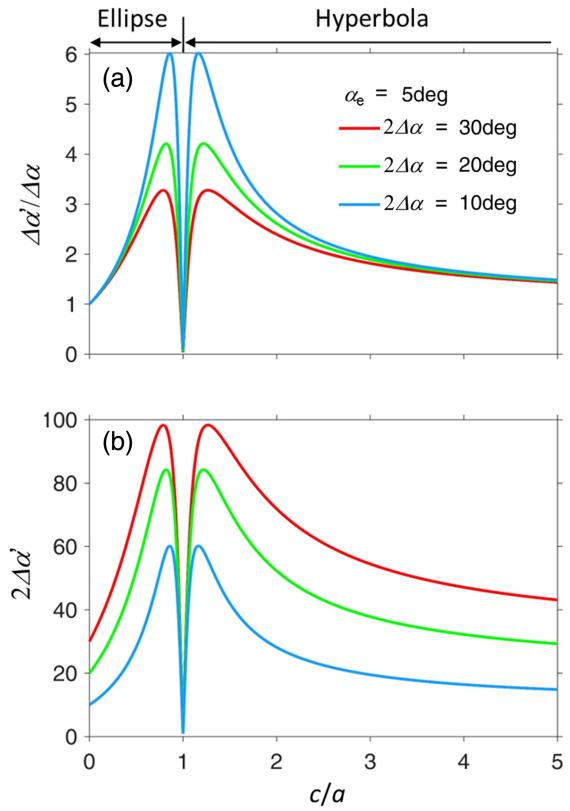

Fig. 2 Variations of (a) magnification ratio $\Delta\alpha'/\Delta\alpha$ and (b) output angular aperture $2\Delta\alpha'$ with eccentricity c/a for different input angular apertures $2\Delta\alpha = 10$ deg, 20 deg, and 30 deg and a fixed edge angle $\alpha_e = 5$ deg.

$\Delta\alpha$ decreases, while Fig. 2(b) shows that the output angular aperture $2\Delta\alpha'$ increases as the input angular aperture $2\Delta\alpha$ increases. This indicates first, the need to optimize ellipsoidal and hyperbolic mirrors for the optimal conditions, especially when the input angular aperture is small; second, even with the optimal conditions, a large input angular aperture is preferred for a larger optimal output angular aperture.

2.2 fs-PW Laser in the Focal Region

Based on the optimal focusing condition for a $2\Delta\alpha = 20$ deg input angular aperture and a $\alpha_e = 5$ deg edge angle, i.e., the optimal output angular aperture $2\Delta\alpha'_{\text{opt}} = 84.3$ deg and optimal eccentricity $c/a_{\text{opt}} = 1.218$ for a hyperbola, the focused field of a typical fs-PW laser is numerically simulated. The fs-PW laser is assumed to have a Gaussian spectrum with a 60 nm FWHM bandwidth centered at 800 nm, which corresponds to the current Ti:sapphire fs-PW lasers.[20–22] The focusing model by Wolf et al.[23] is used in the simulation and given in Appendix B, and therefore the field in the focal region is assumed to come from a cutoff portion of a uniform spherical wave. Another Cartesian coordinate system of $x' - y' - z'$ is set up at the geometrical focus where the z'–axis is the beam propagation direction. Figures 3(a) and 3(d) show the intensity distributions of the laser center wavelength of $\lambda = 800$ nm in the $x' - z'$ focal region for the input and output angular apertures of $2\Delta\alpha = 20$ deg and $2\Delta\alpha' = 84.3$ deg, and the spatial coordinates are normalized by the laser center wavelength $\lambda = 800$ nm. The focal spot size (FWHM) is reduced from about 3.12 to 0.88 λ, and meanwhile, the focal depth (FWHM) decreases from about 61 to 3.8 λ, which agrees well with the results in Fig. 3(b) of Ref. 23. Figures 3(b) and 3(c) show the spatiospectral intensity distribution $I(f, x', z' = 0)$ and spatiotemporal intensity distribution $I(t, x', z' = 0)$ of the pulsed beam in the geometrical focal plane $z' = 0$ for $2\Delta\alpha = 20$ deg, and Figs. 3(e) and 3(f) show the results for $2\Delta\alpha' = 84.3$ deg. During the magnification of angular apertures (from 20 deg to 84.3 deg), the spectral and temporal properties of the pulsed beam at the geometrical focal plane remain unchanged, except for a spatially smaller focal spot. This result shows that secondary focusing using rotational hyperbolic mirrors can reduce the focal spots of current fs-PW lasers to a single-wavelength size. The problem, however, is that the focal depths are also significantly reduced, which makes it challenging to accurately adjust the targets' positions.

2.3 λ^3 Laser in the Focal Region

Realizing the λ^3 regime or the λ^3 laser has always been the way forward for the ultra-intense ultrashort lasers. We keep the magnified angular aperture $2\Delta\alpha'_{\text{opt}} = 84.3$ deg unchanged and broaden the spectral bandwidth to 600 nm (FWHM), with a 12-order super-Gaussian profile and a 600 to 1200 nm FWHM spectral range. Figure 4(a) shows the electric-field distributions of 1200, 900, and 600 nm monochromatic waves in the x'-z' focal region, and Fig. 4(b) shows the corresponding intensity distributions. Due to the ultrabroadband bandwidth with one octave, the distribution in the focal region clearly depends on the spectrum, and the spatial profile increases with increasing wavelength. The focal spot sizes (FWHM) of 1200, 900, and 600 nm waves are about 1.05, 0.79, and 0.53 μm, respectively, and the corresponding focal depths (FWHM) are about 4.65, 3.50, and 2.31 μm, respectively. The focal spot size and the focal depth remain unchanged at about 0.88 and 3.8 λ, respectively, although the absolute values are different for different waves. The spatiospectral intensity distribution $I(f, x', z' = 0)$ in the geometrical focal plane $z' = 0$, as shown in Fig. 4(c), also clearly illustrates the spectral dependence. After the Fourier transform from spectral frequency to time, the spatiotemporal

Table 1 Optimal focusing conditions for different input angular apertures.*

Input angular aperture $2\Delta\alpha$	Optimal eccentricity (for ellipse) c/a_{opt}	Optimal eccentricity (for hyperbola) c/a_{opt}	Optimal magnification ratio $\Delta\alpha'_{\text{opt}}/\Delta\alpha$	Optimal output angular aperture $2\Delta\alpha'_{\text{opt}}$
10 deg	0.859	1.164	6.0	60.0 deg
20 deg	0.821	1.218	4.2	84.3 deg
30 deg	0.790	1.266	3.3	98.4 deg

*The edge angle is fixed at $\alpha_e = 5$ deg.

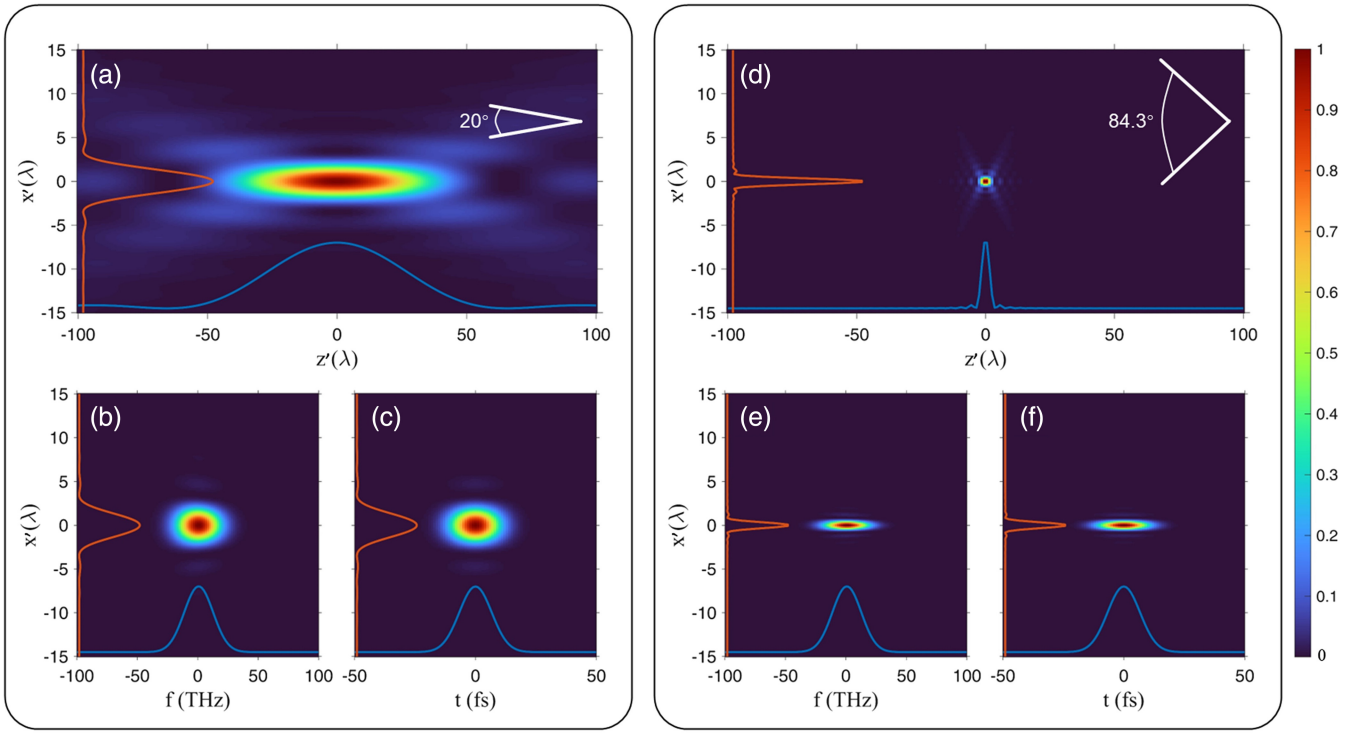

Fig. 3 When the angular apertures are (a)–(c) 20 deg and (d)–(f) 84.3 deg, (a) and (d) spatial intensity distribution in the focal region for the $\lambda = 800$ nm laser center wavelength, and (b) and (e) spatiospectral and (c) and (f) spatiotemporal intensity distributions in the geometrical focal plane $z' = 0$ for a 60 nm FWHM bandwidth Gaussian-pulsed beam. Curves are on-axis profiles.

intensity and electric-field distributions $I(t, x', z' = 0)$ and $U(t, x', z' = 0)$ of the pulsed beam in the geometrical focal plane $z' = 0$ are shown in Figs. 4(d) and 4(e), which have symmetrical profiles in both space and time. The FWHM spatiotemporal size is about 0.73 μm × 3.4 fs, which meets the definition of the λ^3 regime or the λ^3 laser.[1,3] The numerical simulation shows that the combination of a rotational parabolic mirror and a rotational hyperbolic mirror provides a way to enhance the current ultra-intense ultrashort lasers to the λ^3 regime or the λ^3 laser when the wavefront errors[24,25] and the spatiotemporal coupling errors[26–30] are removed. In particular, wavefront correction is critical for tight focusing. In the two-step focusing, the planar wavefront enters the first mirror, a parabolic mirror, and then the spherical wavefront enters the second mirror, a hyperbolic or ellipsoidal mirror. In previous experiments using ellipsoidal mirrors,[17,18] near-ideal single-wavelength-sized focal spots have been achieved successfully, indicating that the wavefront control can meet the experimental needs.

3 Discussion and Conclusion

In this article, a method with hyperbolic mirrors is proposed to magnify the angular aperture of focusing, e.g., from 20 deg to 84.3 deg (the f-number from $f/\sim 2.84$ to $f/\sim 0.55$). Since the focal length is still slightly larger than the beam radius, the Debye approximation is valid[23] and the result is not sensitive to polarization.[31–33] In this case, for simplification, the scalar diffraction theory of a finite spherical wave proposed by Wolf et al.[23] is used. In the next-step work, the polarization effect must be considered as the f-number decreases to very small. In addition, the focusing property of parabolic mirrors as boundary conditions for the Stratton–Chu integral[34] has been well studied,[35,36] since almost all current ultra-intense ultrashort lasers use parabolic mirrors as focusing optics. To apply this method to experiments, another next-step work is to study the Stratton–Chu integral with the boundary condition of the combination of a parabolic mirror and a hyperbolic mirror.

Since the optimal output angular aperture is the same for hyperbolic and ellipsoidal secondary focusing mirrors (see Fig. 2) and the ideal focusing of a cutoff portion of a uniform spherical wave is considered, the secondary focusing results are the same for both methods using hyperbolic and ellipsoidal secondary focusing mirrors. However, when the optimal output angular aperture $2\Delta\alpha'_{\text{opt}}$ is increased to much larger than 90 deg, the above two approximations do not hold, and differences would appear, requiring further in-depth study.

Due to the short working distance of the hyperbolic secondary focusing mirror, which is approximately equal to half of the semi-major axis, mirror contamination and protection should be considered in the design and engineering.

When the two-step focusing method using an ellipsoidal secondary focusing mirror was first proposed, a plasma mirror, i.e., an ellipsoidal plasma mirror, was considered for strong-field experiments because the second mirror, an ellipsoidal mirror, is much smaller than the first mirror, a parabolic mirror.[17,18] Here, although the hyperbolic mirror is much larger than the ellipsoidal mirror, the problem of damage still needs to be considered, and even a hyperbolic plasma mirror needs to be used as well.

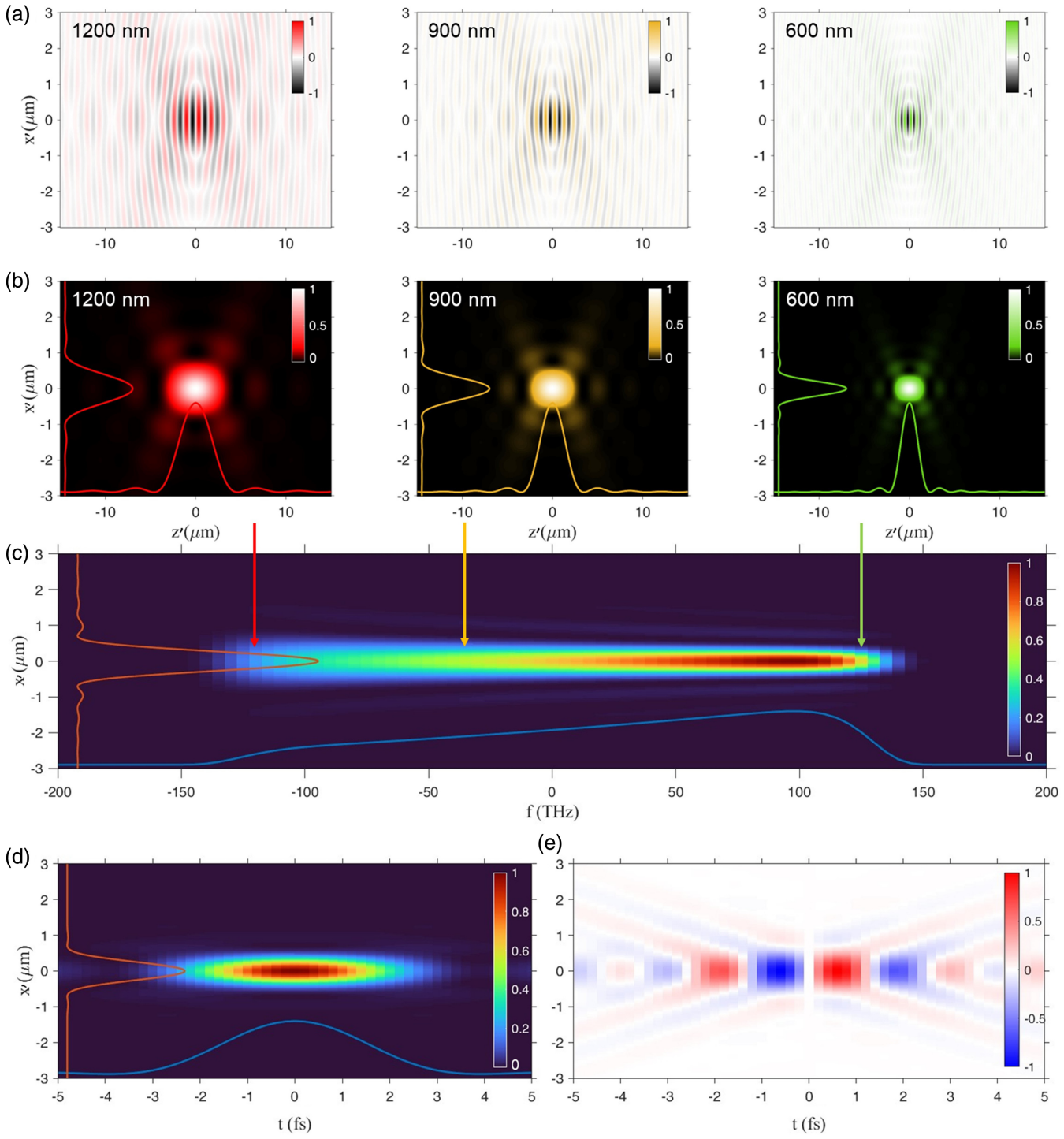

Fig. 4 When the angular aperture is 84.3 deg, spatial (a) electric-field and (b) intensity distributions in the focal region for 1200, 900, and 600 nm wavelengths, and (c) spatiospectral, spatiotemporal (d) intensity and (e) electric-field distributions in the geometrical focal plane $z' = 0$ for a 600 nm FWHM bandwidth 12-order super-Gaussian pulsed beam. Curves are on-axis profiles.

In this article, since the optimal output angular aperture $2\Delta\alpha'_{\text{opt}}$ is not larger than 90 deg, Refs. [31] and [32] show that the optical field is centrosymmetric in the x-x plane, and the distribution along the y axis is not shown. However, when it is increased to much larger than 90 deg, the three-dimensional spatiotemporal optical field needs to be studied in the focal region.

In conclusion, we have proposed that hyperbolic mirrors (another important conic section that also has two foci) can also be used as secondary focusing mirrors after parabolic mirrors to reduce the focal spot size to a single wavelength. Similar to the method using ellipsoidal mirrors, the input large focal spot is located at one focus, while the output small focal spot is

located at the other focus. The difference, however, is that with an ellipsoidal mirror, the input focal spot is a real image, while with a hyperbolic mirror, the input focal spot is a virtual image, which avoids some unwanted strong-field effects in a nonideal vacuum. The optimal focusing condition of this method is presented, and the enhanced tight focusing in a typical fs-PW laser and the λ^3 laser are numerically simulated. This work provides the possibility of achieving single-wavelength-sized focusing for ultra-intense ultrashort lasers, which in turn provides the possibility of realizing the λ^3 regime or the λ^3 laser in the future.

4 Appendix A: Calculation of Angular Aperture Magnification

Because an arbitrary optical ray towards the focus $F_1(-c,0)$ is reflected by the hyperbola to the focus $F_2(c,0)$ [see Fig. 1(b)] and an arbitrary optical ray from the focus $F_1(-c,0)$ is reflected by the ellipse to the focus $F_2(c,0)$ [see Fig. 1(c)], the equations of the two optical rays before and after the reflection are given by

$$\begin{cases} x = \tan\alpha \cdot (z+c) \\ x = \tan\alpha' \cdot (z-c), \end{cases} \tag{1}$$

where α and α' are angles of the incident and reflected optical rays relative to the z axis. Since the two optical rays intersect at the reflection point (Z,X), from Eq. (1) we have the relationship between two angles α and α',

$$\alpha' = \arctan\left(\frac{Z+c}{Z-c}\tan\alpha\right). \tag{2}$$

The hyperbola and ellipse are, respectively, described as

$$\begin{cases} z^2/a^2 - x^2/b^2 = 1 \\ c^2 - a^2 = b^2, \end{cases} \tag{3}$$

and

$$\begin{cases} z^2/a^2 + x^2/b^2 = 1 \\ a^2 - c^2 = b^2, \end{cases} \tag{4}$$

where a and b are semi-major and semi-minor axes, respectively. Because the reflection point (Z,X) is on the hyperbola or ellipse, by substitution of the first equation in Eq. (1) with Eq. (3) or Eq. (4), the horizontal coordinate of the reflection point (Z,X) is given as

$$Z = \frac{-\frac{2c\tan^2\alpha}{a^2-c^2} + \sqrt{\left(\frac{2c\tan^2\alpha}{a^2-c^2}\right)^2 - 4\left(\frac{1}{a^2}+\frac{\tan^2\alpha}{a^2-c^2}\right)\left(\frac{c^2\tan^2\alpha}{a^2-c^2}-1\right)}}{2\left(\frac{1}{a^2}+\frac{\tan^2\alpha}{a^2-c^2}\right)}, \tag{5}$$

which is the same for both an ellipse and a hyperbola.

By substitution of Eq. (5) with Eq. (2), the angle α' of the reflected optical ray becomes a function of the angle α of the incident optical ray, which is also influenced by the parameters a and c, i.e., the eccentricity c/a, of a hyperbola or ellipse. For a beam focused to the focus $F_1(-c,0)$ with an input angular aperture $2\Delta\alpha$ and an edge angle α_e, as shown in Fig. 1, the output angular aperture $2\Delta\alpha'$ at the focus $F_2(c,0)$ can be calculated by $|\alpha'(\alpha_e+2\Delta\alpha)-\alpha'(\alpha_e)|$, and the magnification ratio is given by $|\alpha'(\alpha_e+2\Delta\alpha)-\alpha'(\alpha_e)|/(2\Delta\alpha)$.

5 Appendix B: Simulation of Field Distribution in the Focal Region

Based on the work of Wolf et al.,[23] when a monochromatic, homogeneous, converging spherical wave diffracts at a circular aperture with a radius close to the focal length, the electric-field distribution in the focal region can be described as

$$U(x,z) = -ikA\int_{\cos\Delta\alpha}^{1} \exp(ikzp) J_0\left(kx\sqrt{1-p^2}\right)\mathrm{d}p, \tag{6}$$

where k is the wavenumber, A is a constant amplitude, $\Delta\alpha$ is the angular semi-aperture, z is the propagation axis perpendicular to the circular aperture, x is the vertical axis, and J_0 is the first-kind and zero-order Bessel function.

Disclosures

The authors declare no competing financial interests.

Code and Data Availability

Data and code that support the results of this paper are available from the corresponding author upon reasonable request.

Author Contributions

Z.L. conceived the original concept, initiated the work, conducted the simulation, and wrote the manuscript. Y.Q.L. produced part of figures. Y.X.L. and R.L. supervised the project. Y.Q.L., X.G., Y.X.L., and R.L. discussed the results and contributed to the improvement of the manuscript.

Acknowledgments

This work was supported by the National Key R&D Program of China (Grant No. 2022YFA1604401), the Shanghai Science and Technology Committee Program (Grant Nos. 22560780100 and 23560750200), and the National Natural Science Foundation of China (Grant No. 61925507). Z.L. would like to thank the sponsorship from the Zhangjiang Laboratory.

References

1. G. A. Mourou, T. Tajima, and S. V. Bulanov, "Optics in the relativistic regime," *Rev. Mod. Phys.* **78**(2), 309 (2006).
2. F. Krausz and M. Ivanov, "Attosecond physics," *Rev. Mod. Phys.* **81**(1), 163 (2009).
3. N. M. Naumova et al., "Relativistic generation of isolated attosecond pulses in a λ^3 focal volume," *Phys. Rev. Lett.* **92**(6), 063902 (2004).
4. A. Baltuška, T. Fuji, and T. Kobayashi, "Visible pulse compression to 4 fs by optical parametric amplification and programmable dispersion control," *Opt. Lett.* **27**(5), 306–308 (2002).
5. T. Deckert, A. Vanderhaegen, and D. Brida, "Sub-8-fs pulses in the visible to near-infrared by a degenerate optical parametric amplifier," *Opt. Lett.* **48**(17), 4496–4499 (2023).
6. A. Harth et al., "Two-color pumped OPCPA system emitting spectra spanning 1.5 octaves from VIS to NIR," *Opt. Express* **20**(3), 3076–3081 (2012).
7. G. M. Rossi et al., "Sub-cycle millijoule-level parametric waveform synthesizer for attosecond science," *Nat. Photonics* **14**(10), 629–635 (2020).

8. S. Tóth et al., "Single thin-plate compression of multi-TW laser pulses to 3.9 fs," *Opt. Lett.* **48**(1), 57–60 (2023).
9. A.-L. Viotti et al., "Multi-pass cells for post-compression of ultrashort laser pulses," *Optica* **9**(2), 197–216 (2022).
10. M. Ouillé et al., "Relativistic-intensity near-single-cycle light waveforms at kHz repetition rate," *Light Sci. Appl.* **9**(1), 47 (2020).
11. R. Piccoli et al., "Intense few-cycle visible pulses directly generated via nonlinear fibre mode mixing," *Nat. Photonics* **15**(12), 884–889 (2021).
12. Q. Zhang et al., "Dual-chirped optical parametric amplification for generating few hundred mJ infrared pulses," *Opt. Express* **19**(8), 7190–7212 (2011).
13. Z. Li, Y. Kato, and J. Kawanaka, "Simulating an ultra-broadband concept for Exawatt-class lasers," *Sci. Rep.* **11**(1), 151 (2021).
14. Z. Li, Y. Leng, and R. Li, "Further development of the short-pulse Petawatt laser: trends, technologies, and bottlenecks," *Laser Photonics Rev.* **17**(1), 2100705 (2023).
15. Y. Han et al., "400 nm ultra-broadband gratings for near-single-cycle 100 Petawatt lasers," *Nat. Commun.* **14**(1), 3632 (2023).
16. J. W. Yoon et al., "Realization of laser intensity over 1023 W/cm^2," *Optica* **8**(5), 630–635 (2021).
17. M. Nakatsutsumi et al., "Fast focusing of short-pulse lasers by innovative plasma optics toward extreme intensity," *Opt. Lett.* **35**(13), 2314–2316 (2010).
18. A. Kon et al., "Geometrical optimization of an ellipsoidal plasma mirror toward tight focusing of ultra-intense laser pulse," *J. Phys.: Conf. Ser.* **244**(3), 032008 (2010).
19. Y. Wu, L. Ji, and R. Li, "On the upper limit of laser intensity attainable in nonideal vacuum," *Photonics Res.* **9**(4), 541–547 (2021).
20. W. Li et al., "339 J high-energy Ti:sapphire chirped-pulse amplifier for 10 PW laser facility," *Opt. Lett.* **43**(22), 5681–5684 (2018).
21. F. Lureau et al., "High-energy hybrid femtosecond laser system demonstrating 2 × 10 PW capability," *High Power Laser Sci. Eng.* **8**(4), e43 (2020).
22. Y. Liu et al., "Coherently tiled Ti:sapphire laser amplification: a way to break the 10 petawatt limit on current ultraintense lasers," *Adv. Photonics Nexus* **2**(6) 066009 (2023).
23. W. Wang, A. T. Friberg, and E. Wolf, "Structure of focused fields in systems with large Fresnel numbers," *J. Opt. Soc. Am. A* **12**(9), 1947–1953 (1995).
24. J. I. Kim et al., "Wavefront-corrected post-compression of a 100-TW Ti:sapphire laser," *Opt. Express* **30**(15), 26212–26219 (2022).
25. V. V. Samarkin et al., "Large-aperture adaptive optical system for correcting wavefront distortions of a petawatt Ti:sapphire laser beam," *Quantum Electron.* **52**(2), 187–194 (2022).
26. B. Sun, P. S. Salter, and M. J. Booth, "Pulse front adaptive optics: a new method for control of ultrashort laser pulses," *Opt. Express* **23**(15), 19348–19357 (2015).
27. Z. Li et al., "Degradation of femtosecond petawatt laser beams: spatio-temporal/spectral coupling induced by wavefront errors of compression gratings," *Appl. Phys. Express* **10**(10), 102702 (2017).
28. A. Borot and F. Quéré, "Spatio-spectral metrology at focus of ultrashort lasers: a phase-retrieval approach," *Opt. Express* **26**(20), 26444–26461 (2018).
29. Z. Li and J. Kawanaka, "Complex spatiotemporal coupling distortion pre-compensation with double-compressors for an ultra-intense femtosecond laser," *Opt. Express* **27**(18), 25172–25186 (2019).
30. A. Jeandet et al., "Survey of spatio-temporal couplings throughout high-power ultrashort lasers," *Opt. Express* **30**(3), 3262–3288 (2022).
31. P. Varga and P. Török, "Focusing of electromagnetic waves by paraboloid mirrors. II. Numerical results," *J. Opt. Soc. Am. A* **17**(11), 2090–2095 (2000).
32. T. M. Jeong et al., "Spatio-temporal modification of femtosecond focal spot under tight focusing condition," *Opt. Express* **23**(9), 11641–11656 (2015).
33. X. Zeng and X. Chen, "Characterization of tightly focused vector fields formed by off-axis parabolic mirror," *Opt. Express* **27**(2), 1179–1198 (2019).
34. J. A. Stratton and L. J. Chu, "Diffraction theory of electromagnetic waves," *Phys. Rev.* **56**(1), 99–107 (1939).
35. P. Varga and P. Török, "Focusing of electromagnetic waves by paraboloid mirrors. I. Theory," *J. Opt. Soc. Am. A* **17**(11), 2081–2089 (2000).
36. S. Vallières et al., "Tight-focusing parabolic reflector schemes for petawatt lasers," *Opt. Express* **31**(12), 19319–19335 (2023).

Zhaoyang Li is a professor at Zhangjiang Laboratory, Shanghai, China, with interests in ultra-intense laser technology and engineering. He received his bachelor's, master's, and doctoral degrees from Beijing Institute of Technology, China Academy of Engineering Physics, and Nanjing University of Science and Technology, respectively. He was an assistant professor at Institute of Laser Engineering Osaka University; at Shanghai Institute of Optics and Fine Mechanics, Chinese Academy of Sciences; and at Shanghai Institute of Laser Plasma.

Yanqi Liu is an associate professor at Zhangjiang Laboratory, Shanghai, China, with interests in ultra-intense laser technology and engineering. He received his bachelor's and master's degrees from Changchun University of Science and Technology in 2007 and 2011, respectively. He was a research assistant, research associate, and associate professor at Shanghai Institute of Optics and Fine Mechanics, Chinese Academy of Sciences from 2011 to 2022.

Xiaoyang Guo is an associate professor at Shenzhen Technology University, Guangdong, China, with interests in femtosecond laser technology and engineering. He received his bachelor's and doctoral degrees from Central South University and Shanghai Institute of Optics and Fine Mechanics in 2010 and 2015, respectively. He was a postdoc in Kyoto University and Osaka University from 2015 to 2018.

Yuxin Leng is a professor at Shanghai Institute of Optics and Fine Mechanics (SIOM), Chinese Academy of Sciences (CAS), Shanghai, China, with interests in ultra-intense lasers and physics. He received his bachelor's and doctoral degrees from Wuhan University and SIOM, CAS in 1997 and 2002, respectively. He is an assistant/associate/full professor at SIOM, CAS; director of State Key Laboratory of High Field Laser Physics, SIOM, CAS; and vice-director of SIOM, CAS.

Ruxin Li is a professor at SIOM, CAS, Shanghai, China, with interests in ultra-intense lasers and physics. He received his bachelor's and doctoral degrees from Tianjin University and SIOM, CAS, in 1990 and 1995, respectively. He was elected as a fellow of Optica (formerly OSA) in 2014, Academician of CAS in 2017, and Academician of Third World Academy of Sciences in 2021.